Sensors & Actuators: B. Chemical 424 (2025) 136889

Contents lists available at ScienceDirect

Sensors and Actuators: B. Chemical

journal homepage: www.elsevier.com/locate/snb

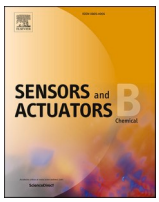

Graphene-based chemiresistive hydrogen sensor for room temperature operation

Cao Tang [a], Wei Jin [a], Xue Xiao [a], Xin Qi [a], Yanqing Ma [a,b,c,*], Lei Ma [a,b,*]

[a] Tianjin International Center for Nanoparticles and Nanosystems, Tianjin University, Tianjin 300072, PR China
[b] Tianjin key laboratory for advanced electronic materials and instrumentation, Tianjin 300072, PR China
[c] School of Precision Instrument and Opto-electronics Engineering, Tianjin University, Tianjin 300072, PR China

ARTICLE INFO

Keywords:
Single layer graphene
Hydrogen sensors
Ultraviolet irradiation
PMMA molecular sieves
Humidity resistance

ABSTRACT

Taking advantage of ultraviolet (UV) irradiation to clean the surface and tuning the charge carriers of graphene, n-doped graphene shows excellent hydrogen sensing capabilities. With assistance of a 265 nm UV light irradiation, the response time of sensor reaches 3 s to 5 ppm hydrogen. And after being relented in ambient condition for a year, it still maintains nearly identical performance. Furthermore, by adding PMMA layer as molecular sieve, the sensor can effectively shield against humidity changes, exhibiting high selectivity towards hydrogen. When the relative humidity varies within the range in 20–70 %, the sensor basically maintains similar response performance. This work streamlines the preparation process of hydrogen sensors and introducing exceptional selectivity with the help of a molecular sieve, facilitating the practical application of hydrogen sensors.

1. Introduction

Hydrogen is recognized as one of the most promising environment friendly and renewable energy sources, with combustion yielding only water as its by-product. It is increasingly regarded as the key alternative to traditional fossil fuels, playing an ever-growing pivotal role in both industrial production and daily life [1,2]. However, hydrogen poses intrinsic challenges: it is extremely flammable, and when the volume fraction exceeds 4 % in air, it can explode instantly with any sparks [3]. Additionally, it is colorless and odorless, which is hardly perceived upon leakage [4]. Consequently, it is vital to have high-performance hydrogen sensors for environmental hydrogen concentration monitoring which can be used for almost all hydrogen usage related industry [5].

At present, the commercialized hydrogen sensors include resistive, electrochemical, thermoelectric, and optical ones [6–9]. Among them, resistive hydrogen sensors have made great progress benefiting their high efficiency, low cost, and simplicity of signal processing [10]. Classical types of such sensors include metal oxide semiconductor (MOS) hydrogen sensors and palladium based (Pd) hydrogen sensors [11,12]. They still face some serious issues in use. For instance, most MOS hydrogen sensors require high operating temperatures [13], and most Pd-based hydrogen sensors suffer from poor long-term stability due to significant volume expansion upon hydrogen absorption [14]. What's more, the response time of these two types of hydrogen sensors is relatively long [15].

To resolve the issues in traditional hydrogen sensors, researchers have experimented with fabricating hydrogen sensors using two-dimensional materials [16,17]. Among these materials, graphene, with its high specific surface area, excellent electrical conductivity (electron mobility over 15000 $cm^2 V^{-1} s^{-1}$ at room temperature) [18], and stable mechanical and chemical properties, is considered as one of the most promising gas sensing materials [19]. The interaction between intrinsic graphene and hydrogen is relatively weak. Most of the graphene-based hydrogen sensors reported rely on the modification using other materials to achieve hydrogen sensing [20,21]. Commonly used modification materials include substances that interact strongly with hydrogen, such as metal nanoparticles [22,23], metal oxide nanoparticles[24,25], and conductive polymers [26]. Wang et al. decorated RGO with WO_3 nanosheets and Pb nanoparticles by microwave-assisted hydrothermal method [27]. The sensor has a response of 94.6–0.05 % hydrogen with a response time of 6 s at 100 ℃. Duan et al. synthesized Pd-SnO_2/RGO ternary nanocomposites with porous structure by hydrothermal method [28]. The sensor exhibited a response time of 25.8 s for 200 ppm hydrogen and a response of 32.8 % at 360 ℃. Although graphene modified shows improved responsiveness to hydrogen, the device fabrication process becomes overly complicated, and the modification

* Corresponding authors at: Tianjin International Center for Nanoparticles and Nanosystems, Tianjin University, Tianjin 300072, PR China.
E-mail addresses: mayanqing@tju.edu.cn (Y. Ma), lei.ma@tju.edu.cn (L. Ma).

https://doi.org/10.1016/j.snb.2024.136889
Received 2 June 2024; Received in revised form 24 October 2024; Accepted 2 November 2024
Available online 2 November 2024

increases the cost. Some of these sensors still require high temperature to perform optimally in hydrogen sensitivity.

There are few reports of the use of graphene alone as hydrogen-sensitive material. Although the response of graphene to hydrogen has also been mentioned in some reports [29–31], their response was rather low and responses speed were slow, serving merely as a reference for performance enhancement. Previous reports have focused on modifying graphene with specific materials to leverage the advantages of graphene in hydrogen sensing. Recently, ultraviolet irradiation has emerged as an effective strategy to enhance the sensitivity of MOS gas sensors [32,33]. Similarly, UV irradiation also significantly impacts graphene. It not only alters the adsorbates on surface of graphene [34], but also enables controlled and reversible modulation of its electronic states [35]. This study endeavors to replace traditional modification methods with photonic activation, exploring the hydrogen sensitivity capabilities of graphene.

Herein, single-layer graphene prepared by Chemical Vapor Deposition (CVD) without modification exhibits significant and rapid response to hydrogen gas under the illumination with 265 nm UV lamp. Specifically, when exposed to 40 ppm of hydrogen, the response time is only 10 seconds, with a response of 3.52 %. Additionally, the sensor still maintains its original response performance after one year. Transferring the PMMA hydrogen molecular sieve to the surface of the graphene significantly enhances the device's resistance to moisture. The simple fabrication process and the ultimate selectivity demonstrated in this work lay a solid foundation for the practical application of graphene-based hydrogen sensors.

2. Experimental

To study the doping state of graphene under various conditions, the hydrogen sensor uses a graphene field-effect transistor (GFET) structure. No gate voltage is applied during the testing of hydrogen sensitivity. The device fabrication process is illustrated in Fig. 1.

2.1. Fabrication of Hydrogen Sensors

Graphene is prepared using the atmospheric pressure chemical vapor deposition method [36]. PMMA-supported graphene is obtained by wet transfer for the preparation of sensors. As shown in Fig. 1 Process I, ① is the copper foil, ② is the graphene grown on the copper foil, ③ is the spin-coated PMMA, and ④ is the PMMA-supported graphene. The source, drain, gate and gate dielectric layers are fabricated on silicon wafers with oxide layers by microfabrication. The graphene is then transferred to it, and the graphene is patterned to obtain GFET. As depicted in Fig. 1 Process II, ⑤ is a silicon wafer with an oxide layer, ⑥ is the silicon wafer with source, drain, gate electrodes and alumina dielectric layer, ⑦ is the transfer of graphene onto the substrate, ⑧ is the completed GFET. Detailed preparation procedures and parameters can be found in the supporting information.

Several studies have reported the relatively high diffusion rate of hydrogen in PMMA layer [37]. To minimize the signal interference caused by changes in air humidity on the hydrogen sensor, PMMA film is selected to enhance the moisture resistance of the sensor. PMMA (Micro Chem, 495A4, 6000 rpm) is spin-coated onto copper foil and baked at 70 ℃ for 10 minutes. The copper foil with PMMA was then placed in potassium persulfate etchant until the copper was etched away, after which the PMMA was transferred onto the fabricated device and baked at 70 ℃ for 30 minutes. As shown in Fig. 1 Process III, ⑨ is the copper foil, ⑩ is the spin coated PMMA on the copper foil, ⑪ is the PMMA film, and ⑫ is the transfer of the PMMA film onto the GFET channel.

2.2. Sensing Test Equipment

The sensing tests were conducted in a home-built chamber, as illustrated in Fig. 2. The interior of the chamber includes a UV lamp (wavelength of 265 nm, with a fixed optical power density of 13 mW/cm^2) and a humidity sensor. There is a micropump at the exit of the chamber. The gases used for testing include target gases, high-purity nitrogen and air with adjustable humidity. The target gases were obtained by diluting gas source cylinders, including 1000 ppm hydrogen, 10,000 ppm ammonia, 100 % methane, 10,000 ppm nitrogen dioxide and 10,000 ppm carbon monoxide. The gases were then diluted to the required test concentrations using flow meters. When studying the

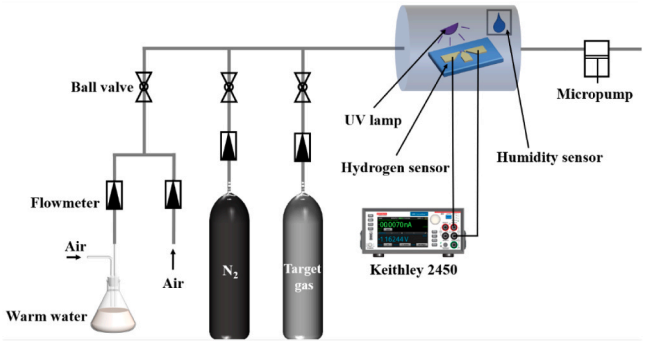

Fig. 2. Schematic diagram of gas sensing test device.

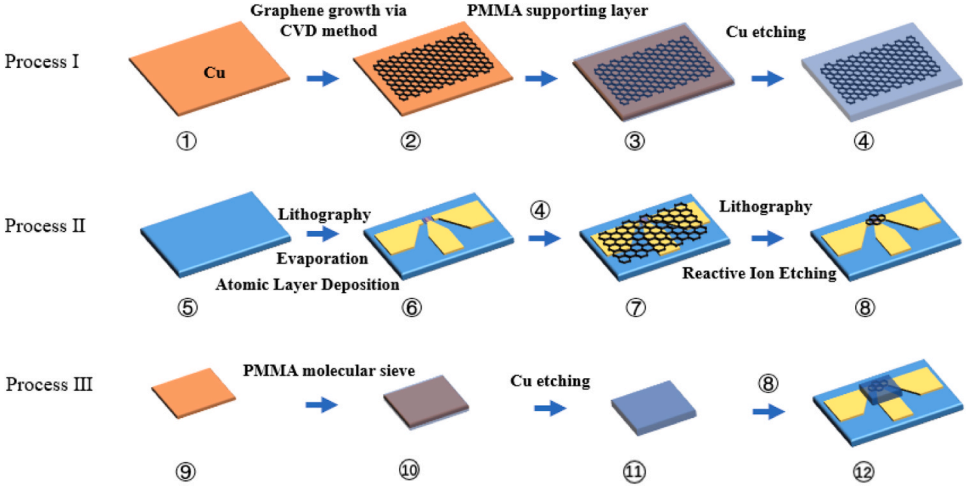

Fig. 1. Schematic of the fabrication process for the graphene gas sensor.

hydrogen sensitivity of bare graphene under UV irradiation, due to significant fluctuations in laboratory air humidity across different seasons and times, and considering the long duration of gas sensing tests coupled with pure graphene's susceptibility to environmental disturbances, we employ high-purity nitrogen as the carrier gas to ensure the reliability of our tests. In subsequent tests with devices containing PMMA layer, we used laboratory air with controlled humidity as the carrier gas to test the humidity resistance of the devices. All hydrogen sensing experiments were carried out at ambient laboratory temperature (~20 ℃) at a total gas flow rate of 1000 sccm.

The response of sensor is defined as the change in resistance of the device before and after exposure to the gas with a specific concentration of hydrogen [38]. The response of the device after hydrogen exposure is calculated using Eq. (1):

$$\text{Response}\ (\%) = \frac{R_H - R_0}{R_0} \times 100 \quad (1)$$

Where R_0 represents the initial resistance of the sensor in the carrier gas (nitrogen or air). R_H represents the resistance of the sensor when it is exposed to environmental with a specific concentration of hydrogen. The response time is calculated based on the time it takes for the device to reach 60 % of its maximum response after hydrogen introduction [39]. The detection limit (LOD) of the sensor can be calculated using Eq. (2):

$$\text{LOD} = \frac{3 \times RMS_{noise}}{Sensitivity} \quad (2)$$

Where RMS_{noise} represents the baseline noise level of the response before hydrogen introduction [32].

The RMS_{noise} is calculated using Eq. (3):

$$\text{RMS}_{\text{noise}} = \sqrt{\frac{\sum (a_i - \overline{a})^2}{N-1}} \quad (3)$$

Here a_i represents the individual resistance measurements, $\overline{a}$ is the average resistance, and N is the number of measurements.

3. Results and discussion

3.1. Structural characterization of sensor

Figs. 3(a) and 3(b) show the optical microscope and SEM images of the graphene gas sensor, respectively. The graphene in the channel appears flat and uniform without wrinkles, making it suitable for subsequent characterization and gas sensing tests. Fig. 3(c) displays the Raman characterization results of the graphene in the channel area. Three distinct peaks were observed at 1346 cm^{-1}, 1591 cm^{-1} and 2685 cm^{-1}, corresponding to D peak, G peak and 2D peak, respectively. The area ratio of the D to G peak (I_D/I_G ratio) is commonly used to evaluate the defects and doping in graphene, while, the area ratio of the 2D to G peak (I_{2D}/I_G ratio) for the number of graphene layers [40]. In Fig. 3(c), the I_D/I_G ratio is 0.14, and the I_{2D}/I_G ratio is 3.72, with the 2D peak half-width of 29.05 cm^{-1}. This exhibits a minute contamination introduction during the device fabrication process and the single layer CVD graphene in the device channel. It is critical for gaining high sensor sensitivity since the carrier mobility in single-layer graphene is normally higher than that in multi-layer graphene that makes the carrier transport process more sensitive to impurities [41].

3.2. Electrical performance testing of sensor

Fig. 4 shows the I-V curves and transfer characteristic curves of the GFET. The linear I-V curve in Fig. 4(a) indicates good ohmic contact between graphene and the electrodes. Fig. 4(b) shows the transfer characteristic curve of GFET, which is useful for analyzing the doping characteristics of graphene under different environmental conditions. Without UV irradiation and exposed to air, the electrical neutrality point of graphene is at approximately 2.13 V, indicating p-type doping. Under UV irradiation in a nitrogen atmosphere, the electrical neutrality point shifts to around −3.74 V, indicating n-type doping. When the GFET is covered with a PMMA layer and exposed to UV light in the air, the neutrality point is near 1.49 V, still reflecting p-type doping.

The surface of graphene in air tends to adsorb water and oxygen molecules, which act as electron acceptors, causing p-type doping of graphene [42,43]. Under UV light irradiation in the air or nitrogen, graphene generates electron-hole pairs. These holes then recombine ($h^+ + O_2^- \rightarrow O_2$), leading to the desorption of gas molecules. The excess photogenerated electrons result in n-type doping of graphene [35]. However, after the addition of a PMMA layer, the ester groups in PMMA, being strong electron-withdrawing groups, may extract electrons from graphene [44]. Moreover, the PMMA layer reduces the optical power density of UV light on the graphene surface, affecting the generation of electron-hole pairs, and ultimately restoring the graphene to a p-type doped state.

3.3. H_2 sensing properties

Response time and response are two key parameters for sensors performance evaluation. Fig. 5(a) displays the response curve to 10 ppm hydrogen with and without the UV light assistant. It is evident the critical role of the UV light proper response of sensor to hydrogen. We examined the effects of UV light at 405 nm and 265 nm on hydrogen response at different optical power densities (Fig. S1). For 405 nm UV light, there is no clear correlation with optical power density. For 265 nm UV light, as optical power density increases, response time decreases, but the response lessens. This phenomenon is that rising up the fermi-level of P-doped graphene to the state of lower density position due to its Dirac cone type linear dispersion relationship, consequently, shorting response time with the same amount of hydrogen adsorption. Additionally, UV irradiation causes local heating of the graphene that can accelerate adsorption rate of hydrogen molecules, and further shortening the response time. To optimize response and minimize energy use, we conducted sensitivity tests with 265 nm UV light at 13 mW/cm^2 optical power density.

Fig. 5(b) shows the test results for hydrogen concentrations of 5 ppm, 10 ppm, 20 ppm and 40 ppm. Since hydrogen acts as an electron donor, when it adsorbs onto the surface of graphene, n-type doped graphene

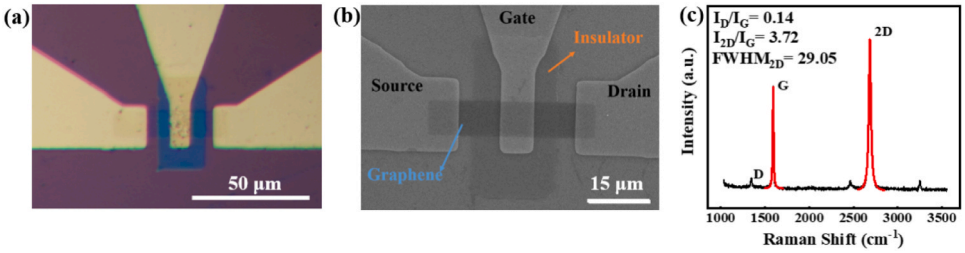

Fig. 3. (a) Light microscope image of GEFT. (b) SEM image of GFET. (c) Raman spectra of graphene at the channel.

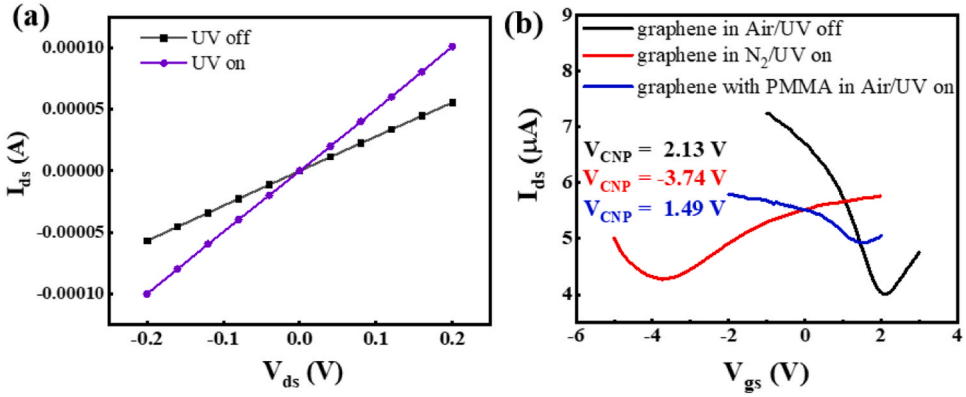

Fig. 4. (a) IV curves of GFET in air with and without UV irradiation. (b) The transfer characteristic curves of GFET in different environments (the black curve indicates that there is no UV light irradiation in the air atmosphere, the red curve indicates the UV light irradiation in the nitrogen atmosphere, and the blue curve indicates the GFET with PMMA protective layer in the air atmosphere and ultraviolet light irradiation).

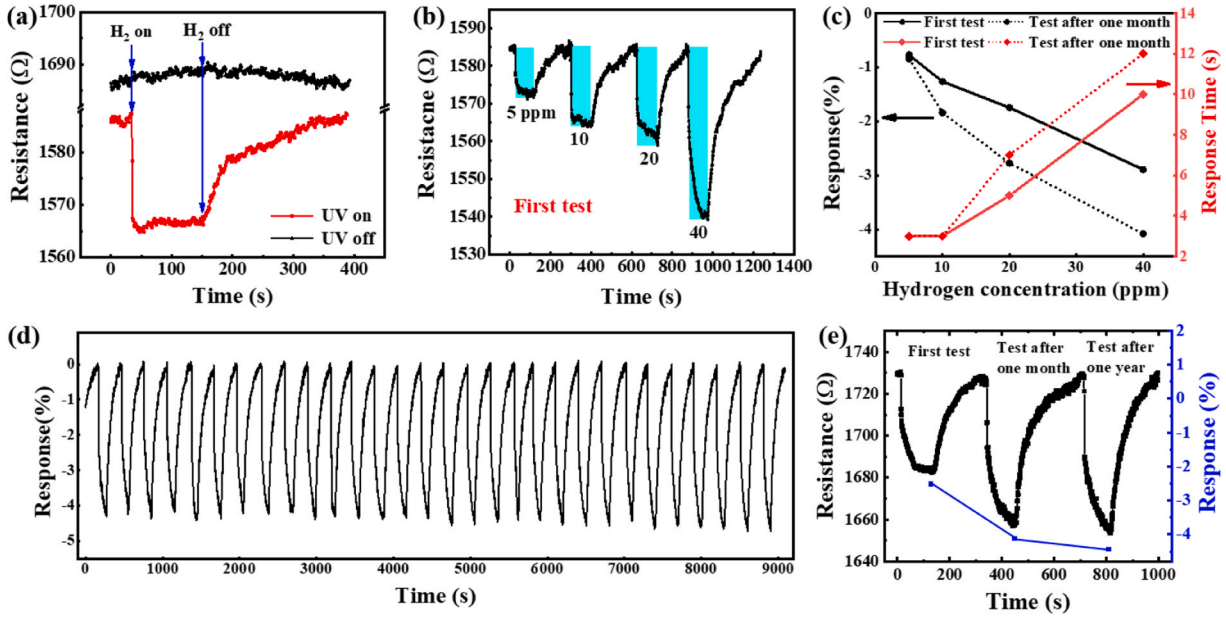

Fig. 5. (a) The response curves of the sensor to 10 ppm H_2 with the UV light turned on and off. (b) The response curves of the sensor to different concentrations of H_2. (c) Changes in response and response time for different concentrations of H_2 during the initial test and after one month. (d) Continuous testing of thirty response curves to 40 ppm H_2 after one year. (e) The changes in the response characteristic curves and response for 40 ppm hydrogen measured during the initial test, one month later, and one year later.

gains electrons, increasing the carrier concentration [45]. As a result, the resistance of graphene decreases when hydrogen is introduced. Moreover, as the concentration of hydrogen gas increases, the response shows a monotonically increase. Multi-cycle tests (Fig. S2 and S3) show consistent responses over continuous testing, indicating good repeatability.

Fig. 5(c) compares the initial and one-month-later responses, revealing minimal variation and confirming stability of graphene. Initial responses were −0.73 %, −1.27 %, −1.75 %, and −2.89 % for increasing concentrations, with times of 3 s, 3 s, 5 s, and 10 s respectively. After one month, these changed to −0.85 %, −1.84 %, −2.77 %, and −4.08 %, with times of 3 s, 3 s, 7 s, and 12 s. This stability and response enhancement relate to defect formation in graphene, confirmed by increased I_D/I_G ratios in Raman spectroscopy (Fig. S4), attributed to UV exposure and aging. These defects enhance gas molecule adsorption and improve response [46], while slightly increasing response time due to additional adsorption sites.

Subsequent tests examine the long-term stability of the sensor. Fig. 5 (d) shows thirty consistent response curves to 40 ppm H_2 after one year, with an average response time of 14 seconds and response of −4.43 %, demonstrating the sensor's repeatability and long-term stability. Fig. 5 (e) summarizes the changes in the response characteristic curves and sensitivity for 40 ppm hydrogen measured during the initial test, after one month, and after one year. The sensor shows a significant response to 40 ppm hydrogen at all these time points, and the response tends to increase over time. These data suggest that the sensor requires an aging process to stabilize its performance during actual use.

In practical applications, the environmental temperature is often variable. Therefore, we explored how changes in resistance due to environmental temperature drift correspond to changes in hydrogen gas concentration in the environment. We first assessed changes in the baseline resistance of sensor across different temperatures, then tested its resistance changes to hydrogen concentrations of 10 ppm, 20 ppm, and 40 ppm at 20 ℃, 40 ℃, 60 ℃, and 80 ℃. Results are summarized in Fig. 6(a) and (b), showing a mild temperature dependence in response. The temperature coefficient of baseline resistance α_T is

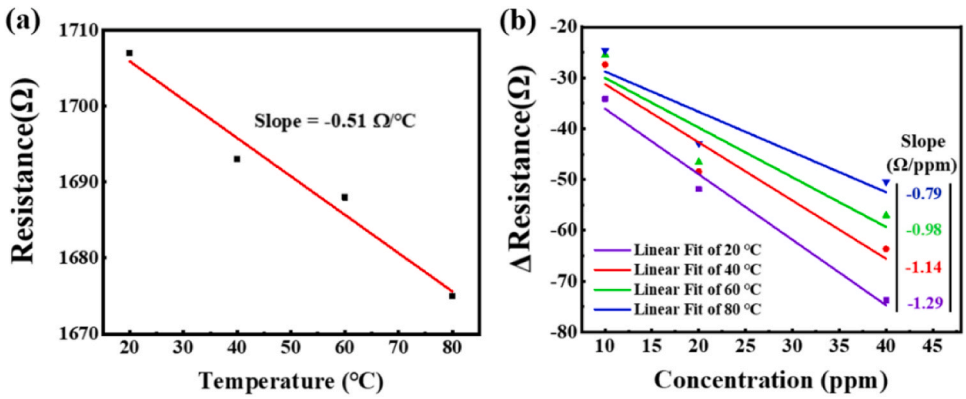

Fig. 6. (a) The trend of baseline resistance changes of the bare graphene device with temperature variations and its linear fitting results. (b) The changes in resistance of the bare graphene device at different temperatures for different concentrations of hydrogen and their fitting results.

$$\alpha_T = \frac{\Delta R_T}{\Delta T} \tag{4}$$

where ΔR_T is the variation of baseline resistance with the change of temperature ΔT. When the measurement is conducted with hydrogen atmosphere, the variation ratio of baseline resistance on hydrogen α_{H2} is

$$\alpha_{H2} = \frac{\Delta R_{H2}}{\Delta [H2]} \tag{5}$$

where ΔR_{H2} is the resistance change after with the hydrogen concentration variation of $\Delta[H2]$. Hence, we can have

$$\frac{\Delta [H2]}{\Delta T} = \frac{\alpha_T}{\alpha_{H2}} \tag{6}$$

From Fig. 6(a), we obtain $\alpha_T = -0.51$ Ω/℃. The values of α_{H2} are −1.29, −1.14, −0.98, and −0.79 Ω/ppm at 20 ℃, 40 ℃, 60 ℃, and 80 ℃, respectively, according to the data shown in Fig. 6(b). Moreover, the calculated values of $\frac{\Delta[H2]}{\Delta T}$ are 0.40、0.45、0.52、0.65 ppm/℃ at temperature of 20 ℃, 40 ℃, 60 ℃, and 80 ℃, respectively.

Fig. 7(a) shows the response curves of the sensor to 5–200 ppm hydrogen, and Fig. 7(b) fits the linear relationship between response and concentration. Within 5–100 ppm, the correlation coefficient R^2 is 0.999 with a slope of 0.0579. By contrast, the slope is 0.0253 in the range of 100–200 ppm. The change in slope is due to the saturation that occurs in most sensors at higher hydrogen concentrations [47]. From baseline noise data, the noise level is calculated at 0.00529. Taking the linear fit slope of 5–100 ppm from Fig. 7(a), the sensitivity at lower concentrations is 0.0579 ppm^{-1}. Based on Eq. (2), the LOD is calculated as 0.27 ppm.

Table 1 summarizes the performance parameters of hydrogen sensors based on two-dimensional materials in recent years. Upon comparison, the hydrogen sensor developed in this work demonstrates the advantage of rapidly detecting extremely low concentrations of hydrogen at room temperature and features a simple fabrication process.

3.4. Improved resistance to moisture and selectivity of sensor

Hydrogen sensors are mostly used in air, where the primary interfering gas is water vapor. Although some graphene gas sensors can operate at high humidity [61], most of them do not account for false signals caused by humidity changes. Due to the relatively small kinetic diameter of hydrogen molecules (0.289 nm) [62], which allows them to pass through PMMA more easily than other gas molecules. Here, we choose PMMA film as molecular sieve to enhance the selectivity of the device towards hydrogen. In this experiment, the PMMA layer with a thickness of 150 nm was selected as the molecular sieve, as detailed in the supporting information Fig. S5 to Fig. S7.

Fig. 8(a) shows the response curves of the graphene gas sensor with and without PMMA layer to humidity changes in the air. Fig. 8(b) shows the response detail before and after the humidity changes. When the relative humidity rises from 15 % to 75 %, the resistance of bare graphene initially increases and then decreases. Initially, the graphene is n-doped (Fig. S8), with electrons as the majority carriers. As the number of water molecules in the environment increases, more water molecules adsorb onto the graphene surface, capturing electrons and reducing the majority carrier concentration in the graphene, thus increasing its resistance[63]. As the water molecules continue to increase, the number of electrons in the graphene decreases until holes become the majority carriers. At this point, the graphene transitions from n-type doping to p-type doping [64]. When additional water molecules adsorb, they continue to capture electrons, increasing the hole concentration, which

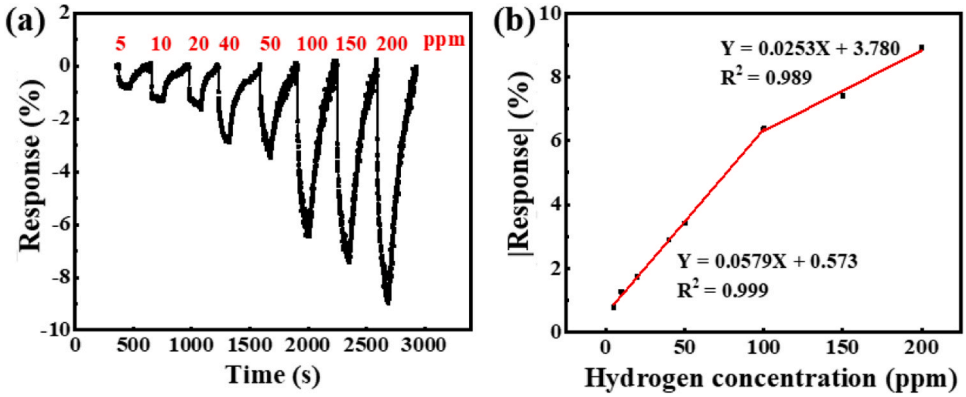

Fig. 7. (a) Response curves of the sensor to different concentrations of hydrogen. (b) Linear fit of response to hydrogen concentration.

Table 1
Performance comparison of H_2 sensors based on two-dimensional materials.

material	operating temperature	response to [H_2]	response time	measurement range	ref
Au/GR	91 ℃	5 % to 500 ppm	1 s	1–1000 ppm	[48]
Pt/rGO	50 ℃	8–0.5 %	63 s	0.3–3 %	[49]
Pd-PANI-rGO	RT	25–1 %	20 s	0.01–2 %	[50]
PdNPs/GR	RT	20–1 %	30 s	0.1–1 %	[22]
Pd/GR	RT	5.88–1 %	180 s	1–4 %	[31]
Pd/GR	RT	NR	18 s	0.02–3 %	[51]
Pd-Ag/GR	190 ℃	5.89 % to 500 ppm	56 s	100–5000 ppm	[52]
SnO_2/GO	20–100 ℃	NR	NR	20–100 ppm	[53]
Au-ZnO/rGO	RT	82 % to 500 ppm	NR	30–500 ppm	[54]
Pd-SnO_2/GR	200 ℃	13–2 %	16 s	2 %	[55]
Pd-ZnO/rGO	50 ℃	35 % to 500 ppm	NR	1 ppb–500 ppm	[56]
Pd-WO_2/GR	RT	NR	13 s	0.05–5 %	[57]
$ZnFe_2O_4$–Pd/rGO	25–100 ℃	11.43 % to 200 ppm	18 s	50–1000 ppm	[47]
Pd/SWCNT	RT	21 % to 1000 ppm	62 s	10–40000 ppm	[58]
3D MoS_2	28–150 ℃	11–1 %	14.3 s	1 %	[59]
Pd/MoS_2	RT	35–1 %	786 s	0.005–1 %	[60]
SLG	RT	3.52 % to 40 ppm	10 s	5–200 ppm	TW
SLG/PMMA	RT	1.06 % to 100 ppm (rh=50 %)	17 s	50–200 ppm	TW

Notes: RT- room temperature. NR-not reported. TW-this work. GR-graphene. GO-graphene oxide. rGO-reduce graphene oxide. SLG-single layer graphene. ref-reference number. SWCNT-single wall carbon nanotube. rh-relative humidity.

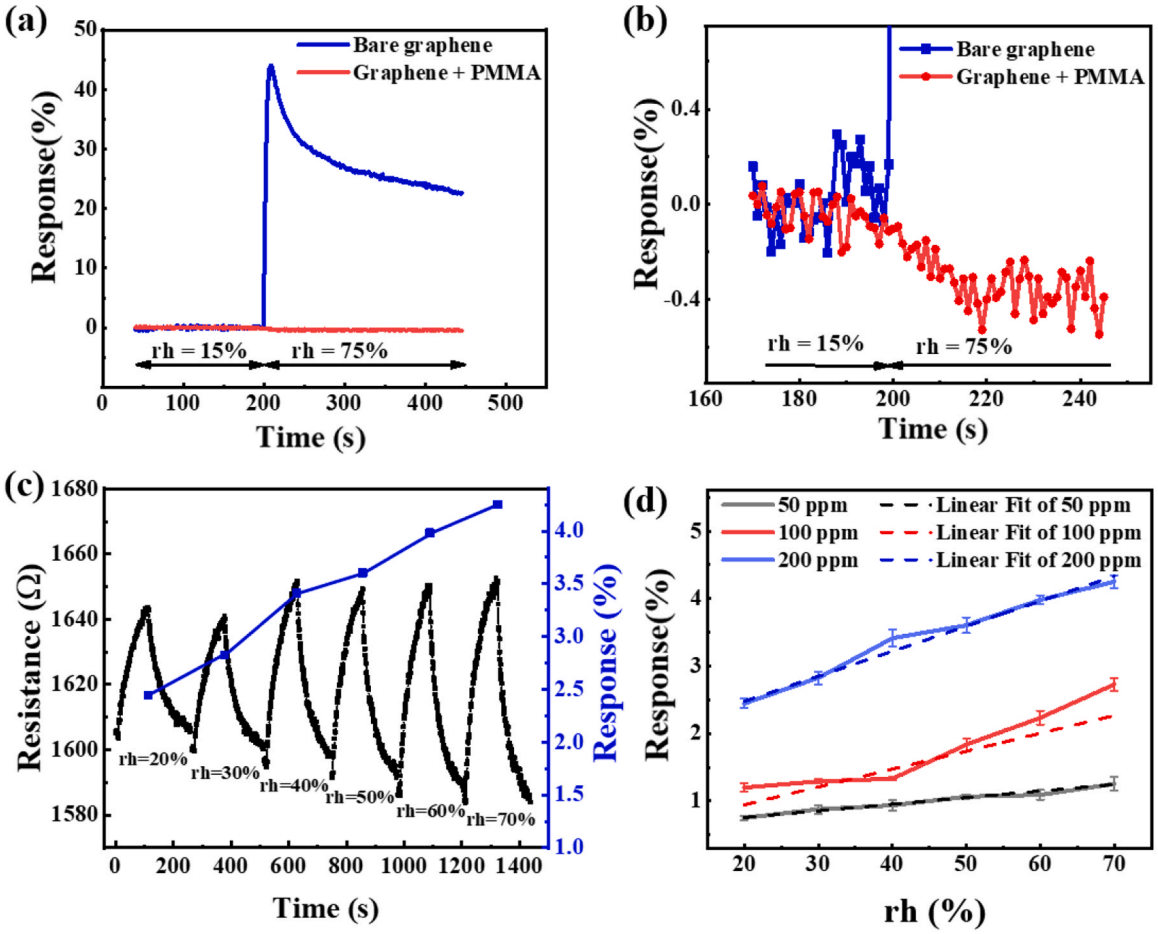

Fig. 8. (a) Response of the bare graphene device with and without PMMA layer when the relative humidity in the air switches from 15 % to 75 %. (b) Detailed responses of the two devices before and after the humidity change. (c) The response characteristic curves and response changes of the device with PMMA layer to 200 ppm hydrogen at different relative humidity levels under UV irradiation (13 mW/cm^2). (d) At different hydrogen concentrations (50 ppm, 100 ppm, 200 ppm), the response of device with PMMA layer varies with humidity.

leads to a decrease in resistance as the majority carrier concentration increases. The response of the sensor without PMMA layer to this change in humidity is as high as 44.05 %, while that of the sensor with the PMMA layer does not exceed 0.6 %, demonstrating PMMA's significant suppression of response to water molecules and minimizing humidity interference during operation.

Fig. 8(c) shows the response characteristic curves and response changes of the device with a PMMA layer to 200 ppm hydrogen under

different relative humidity levels. Fig. 8(d) shows that the response of the device with a PMMA layer to hydrogen increases slightly as humidity increases.

Furthermore, the cyclic stability test is still being conducted in the air atmosphere with a relative humidity of 50 %. Fig. S9 shows the device can maintain a relatively stable response during continuous testing. The impact of adding a PMMA molecular sieve on graphene hydrogen sensors includes: Firstly, the PMMA layer covers some graphene adsorption sites, reducing hydrogen contact and sensor response. Secondly, hydrogen must permeate through PMMA to reach the graphene, delaying response time. Lastly, PMMA lowers the energy density of ultraviolet light on graphene, reducing charge carriers and slowing response speed and sensitivity. While the PMMA layer reduces some performance aspects, it enhances sensor reliability across varying humidity levels, improving adaptability in complex environments.

As shown in Fig. 8(d), we have not completely eliminated the interference caused by humidity changes. We explored how changes in sensor signals due to environmental humidity shifts correspond to changes induced by variations in environmental hydrogen concentrations. Additionally, we have recorded the resistance changes to hydrogen concentrations of 50 ppm, 100 ppm, and 200 ppm under varying humidity, with these results summarized in Fig. 9. Furthermore, several physical quantities are defined to describe "ppm H_2/%rh":

The change rate baseline resistance upon the relative humidity variation in the absence of hydrogen α_{rh} is

$$\alpha_{rh} = \frac{\Delta R_{base}}{\Delta rh} \tag{7}$$

where ΔR_{base} is the baseline resistance change and Δrh is the variation of relative humidity.

The rate of resistance change rate upon relative humidity under a specific concentration of hydrogen α_{H2} is

$$\alpha_{H2} = \frac{\Delta R_{H2}}{\Delta [H2]} \tag{8}$$

where ΔR_{H2} is the resistance change with the hydrogen concentration variation of $\Delta[H2]$.

Therefore,

$$\frac{\Delta [H2]}{\Delta rh} = \frac{\alpha_{rh}}{\alpha_{H2}} \tag{9}$$

α_{rh} is −0.41 Ω/%rh extracted from Fig. 9(a). From Fig. 9(b) we can have the values of α_{H2} at rh=20 %, rh =30 %, rh =40 %, rh =50 %, rh =60 % and rh =70 %are 0.18, 0.21, 0.27, 0.27, 0.30, and 0.31 Ω/ppm, respectively. From these, calculated the values of $\frac{\Delta[H2]}{\Delta rh}$ are −2.28, −1.95, −1.52, −1.52, −1.37, and −1.32 ppm/%rh at rh =20 %, rh =30 %, rh =40 %, rh =50 %, rh =60 % and rh =70 %, respectively.

As depicted in Fig. 10, under ultraviolet light irradiation, the response of sensor to 100 ppm NH_3, 10 % CH_4, 10 ppm NO_2, 50 ppm CO and 100 ppm H_2 is compared with and without PMMA layer. All target gases are obtained by gas cylinders with specific concentrations and diluting them with air to the desired concentration. The relative humidity inside the chamber controlled at 30 % during testing. The results show that the pure graphene sensors without a PMMA molecular sieve exhibit high response to various gases. After the introduction of the PMMA layer, a significant reduction in sensor response to NH_3, CH_4, NO_2 and CO gases was observed. This indicates that the PMMA layer effectively blocks the direct contact of these gas molecules with the graphene. While the response to hydrogen also decreased, the response to hydrogen is the most pronounced, suggesting that the fabricated sensor possesses strong selectivity for hydrogen.

3.5. Gas sensing mechanism

We first discuss the impact of UV irradiation on the electronic states of graphene and gas molecules adsorption. Kelvin Probe Force Microscopy (KPFM) results in Fig. 11(a) show an increase in surface potential and Fermi level of graphene upon UV exposure. Initially, graphene exhibits p-type doping in air, as evidenced by the GFET transfer characteristics in Fig. 4(b), due to electron transfer to adsorbed water vapor and oxygen, making holes the primary charge carriers. UV irradiation generates additional electron-hole pairs [65], leading to the desorption of negatively charged species (such as H_2O^- and O_2^-) from the graphene surface and raising its Fermi level [34]. Under nitrogen atmosphere and UV irradiation at 13 mW/cm^2, graphene exhibits n-type doping, as confirmed in Fig. 4(b). Fig. 11(b) depicts the desorption of water and oxygen under UV light. The triple effect of UV irradiation on graphene sensors includes: First, UV light clears other adsorbed gases from the graphene surface, restoring adsorption sites and cleaning the surface. Second, UV-excited additional charge carriers enhance the sensor's performance [66]. Lastly, UV irradiation promotes hydrogen desorption from the graphene surface, restoring the sensor to its initial state and explaining the observed decrease in response with increased optical power in Fig. S1(a).

The response of pristine graphene to gas molecules is typically explained within the framework of non-covalent electron donor-acceptor interactions [63]. Hydrogen, as an electron donor, increases carrier concentration in n-doped graphene, reducing resistance [35], as shown in Fig. 5. In Fig. 10(a), the response of UV-illuminated graphene to both NH_3 and H_2 is similar because both gases act as electron donors when adsorbed onto the graphene surface. This electron donation alters the charge distribution on the graphene, affecting its conductivity. Since the graphene is not specifically modified, it is plausible that the sensor exhibits comparable responses to both gases. To improve hydrogen selectivity, we added a PMMA layer on the graphene surface. Graphene with PMMA exhibits p-type doping in air, as shown in Fig. 4(b). Upon

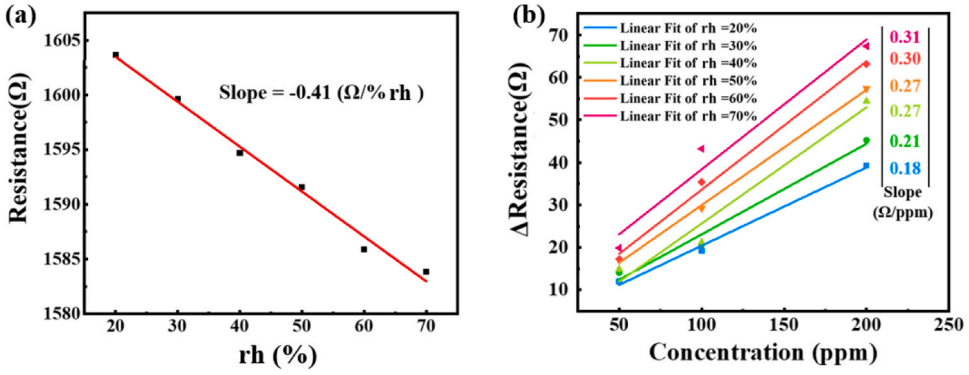

Fig. 9. (a) The trend of the baseline resistance of the device with PMMA layer as humidity changes and its linear fitting results. (b) The changes in resistance of the device with PMMA layer at different humidity levels for various hydrogen concentrations and their fitting results.

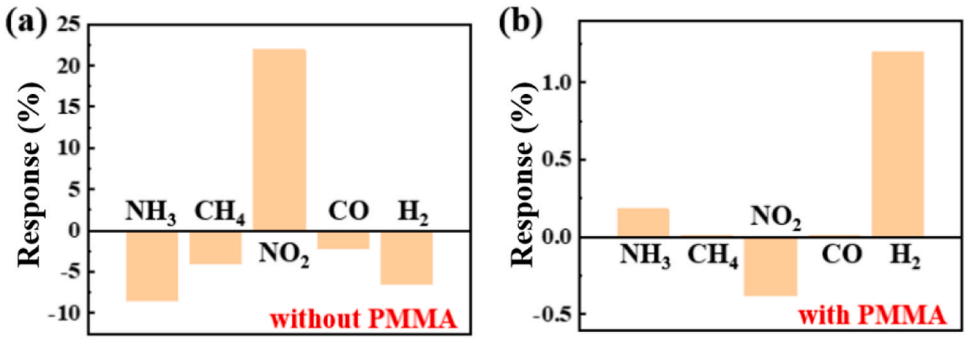

Fig. 10. Comparison of the response results of graphene sensor with (a) and without (b) PMMA molecular sieve to 100 ppm NH_3, 10 % CH_4, 10 ppm NO_2, 50 ppm CO and 100 ppm H_2.

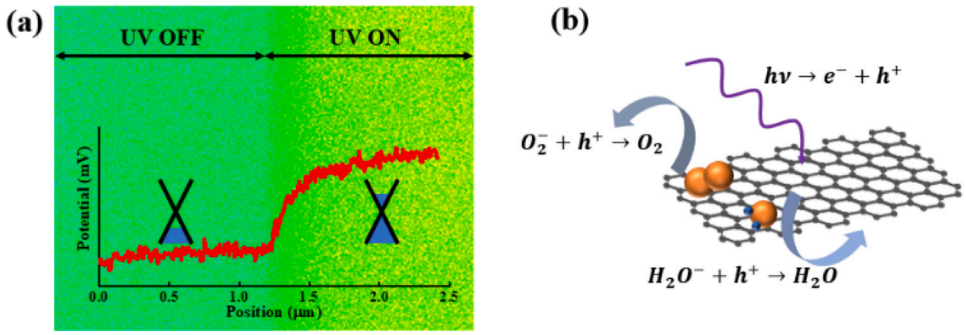

Fig. 11. (a) The surface potential of graphene changes before and after UV light irradiation. (b) Schematic illustration of the desorption of water and oxygen molecules under UV light irradiation.

adsorption of hydrogen, the electron transfer from hydrogen molecules to graphene leads to a decrease in carrier concentration, resulting in an increase in resistance as depicted in Fig. 8(c).

Although PMMA serves as a physical barrier, it exhibits hygroscopic properties. When certain organic materials absorb water molecules, they form water bridges through double hydrogen bonding, resulting in swelling [67,68]. This swelling increases the distance between PMMA chains, leading to the formation of more micropores [69]. These micropores facilitate the diffusion of hydrogen molecules, allowing more hydrogen to penetrate the PMMA layer and reach the graphene surface. As shown in Fig. 8(d), the response of the device with the PMMA layer increases with rising humidity.

4. Conclusion

Using UV light irradiation for a graphene-based hydrogen sensor, it has exceptional sensing capability to low concentrations hydrogen. The response time is 3-second to 5 ppm of hydrogen. After being relented one year, the original response performance still maintained very well. By adding PMMA as the molecular sieve, the sensor exhibits outstanding resistance to moisture. This innovative design harnesses the unique interactive effects of UV light on graphene, shifting away from conventional material modifications to a more nuanced, light-based manipulation. By doing so, it delves into the realm of graphene inherent properties, tapping into its potential as a responsive material for hydrogen detection under light-induced conditions. Future research should explore novel protective coatings to enhance the lifespan and durability of sensor, advancing graphene sensor technology for various applications.

CRediT authorship contribution statement

Wei Jin: Investigation, Data curation. **Cao Tang:** Writing – original draft, Methodology, Investigation, Data curation. **Xin Qi:** Methodology, Data curation. **Xue Xiao:** Data curation. **Lei Ma:** Writing – review & editing, Supervision, Methodology, Funding acquisition, Formal analysis, Data curation, Conceptualization. **Yanqing Ma:** Writing – review & editing, Supervision, Methodology.

Declaration of Competing Interest

The authors declare that they have no known competing financial interests or personal relationships that could have appeared to influence the work reported in this paper.

Acknowledgements

This work was financially supported by the National Key R&D Program of China (No. 2022YFC3006303).

Appendix A. Supporting information

Supplementary data associated with this article can be found in the online version at doi:10.1016/j.snb.2024.136889.

Data Availability

Data will be made available on request.

References

[1] B.M. Opeyemi, Path to sustainable energy consumption: the possibility of substituting renewable energy for non-renewable energy, Energy 228 (2021) 120519.
[2] N. Sazali, Emerging technologies by hydrogen: a review, Int. J. Hydrog. Energy 45 (2020) 18753–18771.
[3] C. Tarhan, M.A. Cil, A study on hydrogen, the clean energy of the future: hydrogen storage methods, J. Energy Storage 40 (2021) 102676.

[4] X.H. Li, Z.Y. Han, R.R. Zhang, Y. Zhang, L.Y. Zhang, Risk assessment of hydrogen generation unit considering dependencies using integrated dematel and topsis approach, Int. J. Hydrog. Energy 45 (2020) 29630–29642.

[5] S. Foorginezhad, M. Mohseni-Dargah, Z. Falahati, R. Abbassi, A. Razmjou, M. Asadnia, Sensing advancement towards safety assessment of hydrogen fuel cell vehicles, J. Power Sources 489 (2021) 229450.

[6] A.K. Pathak, S. Verma, N. Sakda, C. Viphavakit, R. Chitaree, B.M.A. Rahman, Recent advances in optical hydrogen sensor including use of metal and metal alloys: a review, Photonics 10 (2023) 122.

[7] C.M. Wu, K.G. Motora, G.Y. Chen, D.H. Kuo, N.S. Gultom, Highly efficient MoS_2/Cs_xWO_3 nanocomposite hydrogen gas sensors, Front. Mater. 9 (2022) 831725.

[8] Y. Yu, Z.Y. Hu, S.Y. Lien, Y.M. Yu, P. Gao, Self-powered thermoelectric hydrogen sensors based on low-cost bismuth sulfide thin films: quick response at room temperature, ACS Appl. Mater. (2022) 47696–47705.

[9] M. Cho, T. Kim, I. Cho, M. Gao, K. Kang, D. Yang, I. Park, Nanogap formation using a chromium oxide film and its application as a palladium hydrogen switch, Langmuir 38 (2022) 1072–1078.

[10] W.T. Koo, H.J. Cho, D.H. Kim, Y.H. Kim, H. Shin, R.M. Penner, I.D. Kim, Chemiresistive hydrogen sensors: Fundamentals, recent advances, and challenges, ACS Nano 14 (2020) 14284–14322.

[11] V. Ambardekar, T. Bhowmick, P.P. Bandyopadhyay, Understanding on the hydrogen detection of plasma sprayed tin oxide/tungsten oxide (SnO_2/WO_3) sensor, Int. J. Hydrog. Energy 47 (2022) 15120–15131.

[12] Y.Y. Dai, H.C. Jiang, X.H. Zhao, J.W. Tian, X.W. Deng, W.L. Zhang, A temperature-stable Pd nanofilm hydrogen sensor with a wheatstone bridge structure, J. Mater. Sci.: Mater. Electron. 34 (2023) 833.

[13] U.T. Nakate, R. Ahmad, P. Patil, Y.T. Yu, Y.B. Hahn, Ultra thin NiO nanosheets for high performance hydrogen gas sensor device, Appl. Surf. Sci. 506 (2020) 144971.

[14] F. Yang, D.K. Taggart, R.M. Penner, Fast, sensitive hydrogen gas detection using single palladium nanowires that resist fracture, Nano Lett. 9 (2009) 2177–2182.

[15] S.H. Cho, J.M. Suh, B. Jeong, T.H. Lee, K.S. Choi, T.H. Eom, T. Kim, H.W. Jang, Fast responding and highly reversible gasochromic H_2 sensor using Pd-decorated amorphous WO_3 thin films, Chem. Eng. J. 446 (2022) 136862.

[16] Z. Meng, R.M. Stolz, L. Mendecki, K.A. Mirica, Electrically-transduced chemical sensors based on two dimensional nanomaterials, Chem. Rev. 119 (2019) 478–598.

[17] I. Sayago, E. Terrado, E. Lafuente, M.C. Horrillo, W.K. Maser, A.M. Benito, R. Navarro, E.P. Urriolabeitia, M.T. Martinez, J. Gutierrez, Hydrogen sensors based on carbon nanotubes thin films, Synth. Met. 148 (2005) 15–19.

[18] A.K. Geim, K.S. Novoselov, The rise of graphene, Nat. Mater. 6 (2007) 183–191.

[19] S.S. Varghese, S.H. Varghese, S. Swaminathan, K.K. Singh, V. Mittal, Two-dimensional materials for sensing: Graphene and beyond, Electronics 4 (2015) 651–687.

[20] M.N. Norizan, N. Abdullah, N.A. Halim, S.Z.N. Demon, I.S. Mohamad, Heterojunctions of rGO/metal oxide nanocomposites as promising gas-sensing materials-a review, Nanomater. -Basel 12 (2022) 2278.

[21] Z.Y. Zhu, X.M. Ma, C.C. Liu, S.M. Liang, S.F. Xu, L. Wang, J.K. Xu, Facile design of flexible Pd nanoclusters sensitized reduced graphene oxide paper film towards hydrogen sensing, Ceram. Int. 49 (2023) 12840–12845.

[22] B. Alfano, T. Polichetti, M.L. Miglietta, E. Massera, C. Schiattarella, F. Ricciardella, G. Di Francia, Fully eco-friendly H_2 sensing device based on Pd-decorated graphene, Sens. Actuat. B Chem. 239 (2017) 1144–1152.

[23] B.H. Chu, C.F. Lo, J. Nicolosi, C.Y. Chang, V. Chen, W. Strupinski, S.J. Pearton, F. Ren, Hydrogen detection using platinum coated graphene grown on SiC, Sens. Actuat. B Chem. 157 (2011) 500–503.

[24] Z. Zhang, X. Zou, L. Xu, L. Liao, W. Liu, J. Ho, X. Xiao, C. Jiang, J. Li, Hydrogen gas sensor based on metal oxide nanoparticles decorated graphene transistor, Nanoscale 7 (2015) 10078–10084.

[25] D. Dutta, S.K. Hazra, J. Das, C.K. Sarkar, S. Basu, Studies on p-TiO_2/n-graphene heterojunction for hydrogen detection, Sens. Actuat. B Chem. 212 (2015) 84–92.

[26] Y.J. Yang, S.B. Li, W.Y. Yang, W.T. Yuan, J.H. Xu, Y.D. Jiang, In situ polymerization deposition of porous conducting polymer on reduced graphene oxide for gas sensor, ACS Appl. Mater. 6 (2014) 13807–13814.

[27] L. Wang, F. An, X.M. Liu, D.Z. Zhang, Z. Yang, Preparation and hydrogen-sensitive property of WO_3/graphene/Pd ternary composite, Chemosensors 11 (2023) 410.

[28] P.Y. Duan, Q.L. Duan, Q.K. Peng, K.Q. Jin, J.H. Sun, Design of ultrasensitive gas sensor based on self-assembled Pd-SnO_2/rGO porous ternary nanocomposites for ppb-level hydrogen, Sens. Actuat. B Chem. 369 (2022) 132280.

[29] L. Al-Mashat, K. Shin, K. Kalantar-Zadeh, J.D. Plessis, S.H. Han, R.W. Kojima, R. B. Kaner, D. Li, X.L. Gou, S.J. Ippolito, W. Wlodarski, Graphene/polyaniline nanocomposite for hydrogen sensing, J. Phys. Chem. C. 114 (2010) 16168–16173.

[30] B. Sharma, J.S. Kim, MEMS based highly sensitive dual FET gas sensor using graphene decorated Pd-Ag alloy nanoparticles for H_2 detection, Sci. Rep. 8 (2018) 5902.

[31] X. Tang, P.A. Haddad, N. Mager, X. Geng, N. Reckinger, S. Hermans, M. Debliquy, J.P. Raskin, Chemically deposited palladium nanoparticles on graphene for hydrogen sensor applications, Sci. Rep. 9 (2019) 3653.

[32] A. Falak, Y. Tian, L. Yan, M. Zhao, X. Zhang, F. Dong, P. Chen, H. Wang, W. Chu, Room temperature detection of NO_2 at ppb level and full recovery by effective modulation of the barrier height for titanium oxide/graphene schottky heterojunctions, Adv. Mater. Interfaces 6 (2019) 1900992.

[33] J. Wang, Y.Q. Shen, X. Li, Y. Xia, C. Yang, Synergistic effects of UV activation and surface oxygen vacancies on the room-temperature NO_2 gas sensing performance of ZnO nanowires, Sens. Actuat. B Chem. 298 (2019) 126858.

[34] Y.J. Lin, J.J. Zeng, Tuning the work function of graphene by ultraviolet irradiation, Appl. Phys. Lett. 102 (2013) 183120.

[35] Z.T. Luo, N.J. Pinto, Y. Davila, A.T.C. Johnson, Controlled doping of graphene using ultraviolet irradiation, Appl. Phys. Lett. 100 (2012) 253108.

[36] P.-C. Shen, Y. Lin, H. Wang, J.-H. Park, W.S. Leong, A.-Y. Lu, T. Palacios, J. Kong, CVD technology for 2-D materials, IEEE Trans. Electron Devices 65 (2018) 4040–4052.

[37] B. Jang, K.Y. Lee, J.S. Noh, W. Lee, Nanogap-based electrical hydrogen sensors fabricated from Pd-PMMA hybrid thin films, Sens. Actuat. B Chem. 193 (2014) 530–535.

[38] D. Gupta, D. Dutta, M. Kumar, P.B. Barman, C.K. Sarkar, S. Basu, S.K. Hazra, A low temperature hydrogen sensor based on palladium nanoparticles, Sens. Actuat. B Chem. 196 (2014) 215–222.

[39] X. Xiao, W. Jin, C. Tang, X. Qi, R. Li, Y. Zhang, W.S. Zhang, X. Yu, X.D. Zhu, Y. Q. Ma, L. Ma, Thermal reduced graphene oxide-based gas sensor for rapid detection of ammonia at room temperature, J. Mater. Sci. (2023) 11016–11028.

[40] A.C. Ferrari, J.C. Meyer, V. Scardaci, C. Casiraghi, M. Lazzeri, F. Mauri, S. Piscanec, D. Jiang, K.S. Novoselov, S. Roth, A.K. Geim, Raman spectrum of graphene and graphene layers, Phys. Rev. Lett. 97 (2006) 187401.

[41] K. Nagashio, T. Nishimura, K. Kita, A. Toriumi, Mobility variations in mono- and multi-layer graphene films, Appl. Phys. Express 2 (2009) 025003.

[42] C. Casiraghi, S. Pisana, K.S. Novoselov, A.K. Geim, A.C. Ferrari, Raman fingerprint of charged impurities in graphene, Appl. Phys. Lett. 91 (2007) 233108.

[43] T.O. Wehling, A.I. Lichtenstein, M.I. Katsnelson, First-principles studies of water adsorption on graphene: the role of the substrate, Appl. Phys. Lett. 93 (2008) 202110.

[44] W.H. Lee, J. Park, Y. Kim, K.S. Kim, B.H. Hong, K. Cho, Control of graphene field-effect transistors by interfacial hydrophobic self-assembled monolayers, Adv. Mater. 23 (2011) 3460–3464.

[45] B.H. Chu, J. Nicolosi, C.F. Lo, W. Strupinski, S.J. Pearton, F. Ren, Effect of coated platinum thickness on hydrogen detection sensitivity of graphene-based sensors, Electrochem. Solid-State Lett. 14 (2011) K43–K45.

[46] A. Gao, P.J. Rizo, E. Zoethout, L. Scaccabarozzi, C.J. Lee, V. Banine, F. Bijkerk, Extreme ultraviolet induced defects on few-layer graphene, J. Appl. Phys. 114 (2013) 044313.

[47] L.S.K. Achary, B. Maji, A. Kumar, S.P. Ghosh, J.P. Kar, P. Dash, Efficient room temperature detection of H_2 gas by novel $ZnFe_2O_4$-Pd decorated rGO nanocomposite, Int. J. Hydrog. Energy 45 (2020) 5073–5085.

[48] Y. Kim, Y.S. Choi, S.Y. Park, T. Kim, S.P. Hong, T.H. Lee, C.W. Moon, J.H. Lee, D. Lee, B.H. Hong, H.W. Jang, Au decoration of a graphene microchannel for self-activated chemoresistive flexible gas sensors with substantially enhanced response to hydrogen, Nanoscale 11 (2019) 2966–2973.

[49] X. Lu, X. Song, C. Gu, H. Ren, Y. Sun, J. Huang, Freeze drying-assisted synthesis of Pt@reduced graphene oxide nanocomposites as excellent hydrogen sensor, J. Phys. Chem. Solids 116 (2018) 324–330.

[50] Y. Zou, Q. Wang, C. Xiang, C. Tang, H. Chu, S. Qiu, E. Yan, F. Xu, L. Sun, Doping composite of polyaniline and reduced graphene oxide with palladium nanoparticles for room-temperature hydrogen-gas sensing, Int. J. Hydrog. Energy 41 (2016) 5396–5404.

[51] J. Ma, Y. Zhou, X. Bai, K. Chen, B.O. Guan, High-sensitivity and fast-response fiber-tip fabry-perot hydrogen sensor with suspended palladium-decorated graphene, Nanoscale 11 (2019) 15821–15827.

[52] B. Sharma, J.-S. Kim, Graphene decorated Pd-Ag nanoparticles for H_2 sensing, Int. J. Hydrog. Energy 43 (2018) 11397–11402.

[53] M.A.H.M. Munasinghe, E. Comini, D. Zappa, N. Poli, G. Sberveglieri, Low temperature gas sensing properties of graphene oxide/SnO_2 nanowires composite for H_2, Procedia Eng. 168 (2016) 305–308.

[54] Q.A. Drmosh, A.H. Hendi, M.K. Hossain, Z.H. Yamani, R.A. Moqbel, A. Hezam, M. A. Gondal, UV-activated gold decorated rGO/ZnO heterostructured nanocomposite sensor for efficient room temperature H_2 detection, Sens. Actuat. B Chem. 290 (2019) 666–675.

[55] S. Dhall, M. Kumar, M. Bhatnagar, B.R. Mehta, Dual gas sensing properties of graphene-Pd/SnO_2 composites for H_2 and ethanol: Role of nanoparticles-graphene interface, Int. J. Hydrog. Energy 43 (2018) 17921–17927.

[56] Y. e Sun, D. Zhang, H. Chang, Y. Zhang, Fabrication of palladium-zinc oxide-reduced graphene oxide hybrid for hydrogen gas detection at low working temperature, J. Mater. Sci.: Mater. Electron. 28 (2016) 1667–1673.

[57] M. Chen, L. Zou, Z. Zhang, J. Shen, D. Li, Q. Zong, G. Gao, G. Wu, J. Shen, Z. Zhang, Tandem gasochromic-Pd-WO_3/graphene/Si device for room-temperature high-performance optoelectronic hydrogen sensors, Carbon 130 (2018) 281–287.

[58] X.W. Li, M. Le Thai, R.K. Dutta, S.P. Qiao, G.T. Chandran, R.M. Penner, Sub-6 nm palladium nanoparticles for faster, more sensitive H_2 detection using carbon nanotube ropes, ACS Sens. 2 (2017) 282–289.

[59] A.V. Agrawal, R. Kumar, S. Venkatesan, A. Zakhidov, Z. Zhu, J.M. Bao, M. Kumar, M. Kumar, Fast detection and low power hydrogen sensor using edge-oriented vertically aligned 3-D network of MoS_2 flakes at room temperature, Appl. Phys. Lett. 111 (2017) 093102.

[60] D.H. Baek, J. Kim, MoS_2 gas sensor functionalized by Pd for the detection of hydrogen, Sens. Actuat. B Chem. 250 (2017) 686–691.

[61] B. Kwon, H. Bae, H. Lee, S. Kim, J. Hwang, H. Lim, J.H. Lee, K. Cho, J. Ye, S. Lee, W.H. Lee, Ultrasensitive N-channel graphene gas sensors by nondestructive molecular doping, ACS Nano 16 (2022) 2176–2187.

[62] J. Hong, S. Lee, J. Seo, S. Pyo, J. Kim, T. Lee, A highly sensitive hydrogen sensor with gas selectivity using a PMMA membrane-coated Pd nanoparticle/single-layer graphene hybrid, ACS Appl. Mater. 7 (2015) 3554–3561.

[63] O. Leenaerts, B. Partoens, F.M. Peeters, Adsorption of H_2O, NH_3, CO, NO_2, and NO on graphene: a first-principles study, Phys. Rev. B. 77 (2008) 125416.

[64] R. Pearce, T. Iakimov, M. Andersson, L. Hultman, A.L. Spetz, R. Yakimova, Epitaxially grown graphene based gas sensors for ultra sensitive NO_2 detection, Sens. Actuat. B Chem. 155 (2011) 451–455.
[65] M. Freitag, T. Low, F.N. Xia, P. Avouris, Photoconductivity of biased graphene, Nat. Photon. 7 (2013) 53–59.
[66] X. Yan, Y.A. Wu, R. Li, C.Q. Shi, R. Moro, Y.Q. Ma, L. Ma, High-performance UV-assisted NO_2 sensor based on chemical vapor deposition graphene at room temperature, ACS Omega 4 (2019) 14179–14187.
[67] Y. Hashimasa, H. Daitoku, T. Numata, Y. Matsuda, Correlation between the swelling characteristics and humidity cycle durability of a polymer electrolyte membrane, J. Electrochem. 75 (2016) 685–694.
[68] Y. Lee, S.-K. Kim, Y.-J. Park, J. Cho, H.-J. Koo, A humidity-sensing composite microfiber based on moisture-induced swelling of an agarose polymer matrix, Polym. Compos. (2019) 3582–3587.
[69] W.P. Kang, Y. Bao, H.L. Wang, N.P. Cao, S.X. Cui, Force-induced enhancement of hydrophilicity of individual polymethyl methacrylate chain, Chin. J. Chem. 41 (2023) 2289–2295.

Cao Tang obtained his bachelor's degree from Tianjin University in 2020. Currently, he is pursuing a Master degree at the Tianjin International Center for Nanoparticles and Nanosystems in Tianjin University. His primary area of research focuses on the development of graphene-based gas sensors.

Wei Jin received his M.S. degree from Harbin Institute of Technology in 2018. Currently, he is a Ph.D. candidate at Tianjin International Center for Nanoparticles and Nanosystems in Tianjin University. His main research interests include Graphene-based gas sensor.

Xue Xiao received her M.S. degree from Tianjin International Center for Nanoparticles and Nanosystems, Tianjin University in 2023. Her project is devoted to research graphene-based ammonia sensors for the early diagnosis of diseases.

Xin Qi obtained his bachelor's degree from Hebei University of Technology in 2019. He is currently pursuing a master's degree at the Tianjin International Center for Nanoparticles and Nanosystems, Tianjin University. His main research focus is on graphene-based biosensors.

Dr. Yanqing Ma received her Ph.D. degree in physical chemistry from Lanzhou Institute of Chemical Physics, CAS in 2009. She joined the International Center for Nanoparticles and Nanosystems in Tianjin University in 2017. Her research focuses on developing two-dimensional catalyst and graphene based energy storage devices and sensors.

Prof. Lei Ma earned his Ph.D. degree in 2010. Then he had his Postdoc training in Brown University and Georgia Tech. From 2016, he took a full professor position in Tianjin University. His research mainly focuses on graphene electronics related physics and cluster physics as well as the instrumentation of mass spectrometer and high resolution photoelectrometer.